Interfacial Assembly and Jamming of Soft Nanoparticle Surfactants into Colloidosomes and Structured Liquids

Beibei Wang,[+a] Bangqi Yin,[+a] Hao Yu,[a] Zhao Zhang,[a] Guan Wang,[a] Shaowei Shi,*[a] Xinggui Gu,*[a, b] Wantai Yang,[a] Ben Zhong Tang,[c] and Thomas P. Russell[d, e]*

[+] *These authors contributed equally to this work.*

[a] Beijing Advanced Innovation Center for Soft Matter Science and Engineering, Beijing University of Chemical Technology, Beijing 100029, China

[b] Beijing National Laboratory for Molecular Sciences, Beijing, 100190, China

[c] School of Science and Engineering, Shenzhen Institute of Aggregate Science and Technology, The Chinese University of Hong Kong (Shenzhen), Shenzhen 518172, China

[d] Department of Polymer Science and Engineering, University of Massachusetts, Amherst, Massachusetts 01003, USA

[e] Materials Sciences Division, Lawrence Berkeley National Laboratory, 1 Cyclotron Road, Berkeley, California 94720, USA

KEYWORDS: Liquid-liquid interfaces, self-assembly, colloidosomes, structured liquids, aggregation-induced emission

ABSTRACT: Nanoparticle surfactant (NPS) offers a powerful strategy to generate all-liquid constructs that integrate the inherent properties of the NPs into 3D architectures. Here, using the co-assembly of fluorescent polymeric nanoparticles and amine-functionalized polyhedral oligomeric silsesquioxane, the assembly and jamming behavior of a new type of NPS at the oil-water interface is uncovered. Unlike "solid" inorganic nanoparticles, "soft" polymeric nanoparticles can reorganize when jammed, leading to a relaxation and deformation of the interfacial assemblies, e.g., the 3D printed sugar-coated haws stick-like liquid tubules. With NPS serving as emulsifiers, stable Pickering emulsions are prepared, that can be converted into robust colloidosomes with pH-responsiveness, showing numerous potential applications for encapsulation and controlled release.

Introduction

Self-assembly has drawn considerable attention for the fabrication of hierarchical, functional structures that span multiple length scales.[1-2] Among these, Pickering emulsions, prepared from the self-assembly of colloidal particles at the interface between two immiscible liquids (e.g., oil and water), offer the ability to enable the compartmentalization of one liquid in another liquid, providing a simple route for encapsulation and release.[3-6] By reinforcing the particle-based interfacial shell, the Pickering emulsion precursor can be converted into robust microcapsules, i.e., colloidosomes, that can survive when the oil and water are removed.[7] Many examples of micron-sized colloidal particles, for example, polystyrene latexes, have been used to stabilize Pickering emulsions, and then to produce colloidosomes.[8-9] Extending the particle size to

nanoscale is particularly attractive since the inherent optical, electronic, and magnetic properties of nanoparticles can be integrated into the assemblies, and the permeability of colloidosomes can be adjusted.[10] However, the small binding energies of the nanoparticles to the interface and the inherent particle size distribution of the nanoparticles lead to assemblies that are liquid-like in nature, i.e. disordered and highly mobile, and that are dynamic with continuous adsorption and the nanoparticles to the interfaces.[11-12] By designing or modifying the nanoparticle surface, the binding energy of nanoparticles to the interface can be increased, e.g., by generating Janus-type nanoparticles with surfaces that are part hydrophobic and part hydrophilic, but this can be done only with detailed preparation or synthesis and the accompanying cost.[13-16]

To circumvent this, using the interactions of functionalized nanoparticles dispersed in one liquid and ligands bearing a complementary functionality dissolved in a second, immiscible liquid can be used.[17] Here, a well-defined number of ligands are anchored to the surface of the nanoparticles to produce nanoparticle surfactants (NPSs) *in situ*, significantly increasing the binding energy of the nanoparticle, leading to the formation of an elastic NPS monolayer at the interface.[18-19] Using NPSs as the emulsifier, stable Pickering emulsions can be easily prepared and, as the systems attempt to reduce the interfacial area, the NPS assemblies jam, locking in any further change in the interfacial area and, therefore, change in the shape of the liquids. If the droplets are deformed, say by applying a shear force, the emulsion droplets can be locked into highly non-equilibrium shapes, i.e. structured emulsions with excellent mechanical strength.[20-22] Exploiting the mechanics of NPS-stabilized interfaces, liquids with more complex geometries can be achieved by using either molding or 3D printing techniques, affording the possibility of constructing all-liquid devices with advanced functions for mass, ion or energy transport or compartmentalized chemical reactions.[23-27] Since the co-assembly strategy is not specific to the

shape or chemical constitution of the nanoparticles, the range of nanoparticles and ligands that can be used to affect NPS formation is quite broad, opening a vast range of potential applications.[28-32]

In this study, we present the formation, assembly and jamming of a new type of NPS, using fluorescent polymeric nanoparticles (FPNPs) and amine-functionalized polyhedral oligomeric silsesquioxane (POSS-NH_2) at the oil-water interface. As shown in Figure 1 and Figure S1-S2, FPNPs (~ 200 nm in diameter with a narrow particle size distribution, polydispersity index (PDI) = 0.09) are prepared by a self-stabilized precipitation (2SP) polymerization,[33-34] where maleic anhydride (MAH), styrene (St), divinyl benzene (DVB), and unilateral 4-vinylbenzyl-modified tetraphenylethylene (TPE-1VBC) were copolymerized in isoamyl acetate. After hydrolyzing the anhydride groups into carboxylic acid groups, FPNPs can be uniformly dispersed in an aqueous medium. Due to the aggregation-induced emission (AIE) characteristic of TPE-1VBC,[35-39] it can be used to monitor the state of aggregation of the FPNPs during interfacial self-assembly process. In comparison to solid inorganic nanoparticles, FPNPs are viscoelastic materials due to the polymeric nature of the particle and, therefore, can reorganize during the compression of the interface to reduce interfacial energy, leading to a relaxation and deformation of the interfacial assemblies. Using the all-liquid 3D printing technique, sugar-coated haws stick-like liquid tubules can be produced. Using Pickering emulsions stabilized by FPNP-based NPS, robust colloidosomes can be achieved by sintering the FPNP monolayer at the interface, which shows pH-controlled release of the water-soluble species within the microcapsules.

Figure 1. Schematic representation showing (a) the preparation of FPNPs and (b) the co-assembly of the FPNPs and POSS-NH_2 at the oil-water interface.

Results and Discussion

Dispersing FPNPs in water phase and dissolving POSS-NH_2 in toluene phase results in the *in situ* formation of NPSs at the toluene-water interface. Prior to understanding the co-assembly kinetics of NPSs at the interface, the interfacial activity of FPNP was investigated at different pH values. As shown in Figure 2a-b, in absence of POSS-NH_2, FPNPs show weak interfacial activity at pH > 4.0, with an equilibrium interfacial tension of ~ 33 mN m^{-1}, closed to that of the pure toluene-water system (~ 36 mN m^{-1}). At pH < 4.0, a reduction in the equilibrium interfacial tension is obtained, indicating the enhanced interfacial activity of FPNP due to the increased degree of protonation of the carboxylic acid groups. At pH = 3.0, when reducing the volume of the pendant droplet to compress the interfacial assemblies after 1200 s, wrinkles are observed at

large compression (Figure 2c and Video S1). The compression is stopped after wrinkling is observed and, it is found that, wrinkles relax rapidly. This compression−relaxation process can be repeated several times until the droplet is fully withdrawn into the needle, indicating the binding energy of FPNP to the interface is too low to withstand the compressive force and FPNPs are ejected from the interface.

With FPNPs dispersed in water against POSS-NH_2 dissolved in toluene, the interfacial activity of FPNP can be significantly enhanced by forming NPSs at the interface. Here, POSS-NH_2 acts as a surfactant due to the hydrophobic POSS segment and hydrophilic amine group, spontaneously segregating to the interface and interacting with FPNPs via electrostatic interactions and forming Janus-like NPSs (Figure S3 and Figure S4). As shown in Figure 2d-e, by varying the pH from 8.0 to 3.0, the equilibrium interfacial tension decreases from 25 to 4.0 mN m^{-1}, indicating the electrostatic interactions between FPNP and POSS-NH_2 are enhanced, which is due to the increased degree of protonation of the amine groups. At pH = 3.0, when compressing the interfacial assemblies after 20 min, wrinkles are observed immediately, indicating the surface coverage of NPSs is quite high (Figure 2f and Video S2). The wrinkles relax slowly in 6.0 min, while the droplet remains the nonequilibrium shape, indicating that the NPSs at the interface reorganize into an assembly with a higher areal density. When compressing the interfacial assemblies again, wrinkles appear again and do no relax after 1 h, indicating a full jamming of the interfacial assembly, preventing the reorganization of NPS assembly. This reorganization behavior is similar to that seen previously with polyelectrolyte surfactants,[40-41] indicating that FPNP can deform under compression due to its intrinsic soft nature, relaxing the interfacial stresses. By withdrawing the droplet into the needle and then reinjecting it to the

initial volume, a highly deformed droplet encapsulated with an elastic film is obtained, demonstrating the ability to re-shape the liquids (Figure 2g and Video S3).

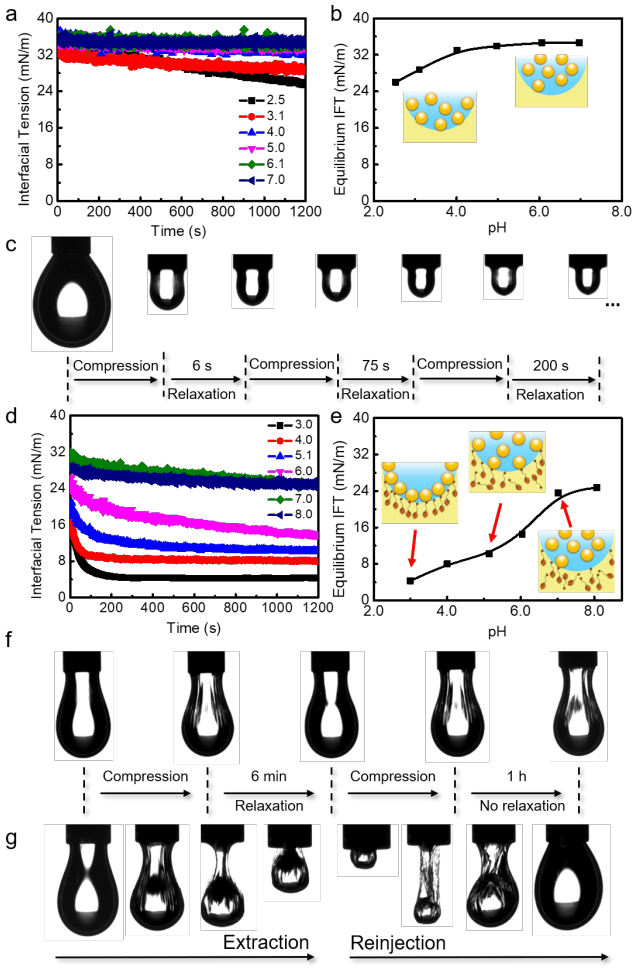

Figure 2. (a) Time evolution of interfacial tension and (b) equilibrium interfacial tension between FPNP aqueous solution and pure toluene with different pH. (c) Snapshots of droplet morphology in repeated compression-relaxation experiments. From (a) to (c), [FPNP] = 0.05 mg mL^{-1}. (d) Time evolution of interfacial tension and (e) equilibrium interfacial tension between FPNP aqueous solution and POSS-NH_2 toluene solution with different pH. (f) Snapshots of droplet morphology in repeated compression-relaxation experiments. (g) Snapshots of droplet's

morphology evolution in an extraction-reinjection process. From (d) to (g), [FPNP] = 0.05 mg mL^{-1}, [POSS-NH_2] = 0.1 mg mL^{-1}.

Due to the incorporation of the AIE-active TPE-1VBC, yellow fluorescence at 565 nm can be observed from the FPNPs, and the formation and assembly of NPSs at the interface can be visualized in real-time by laser scanning confocal microscope (LSCM). As shown in Figure 3a, when placing a water droplet with dispersed FPNPs (0.05 mg mL^{-1}, pH 3.0) into toluene solution of POSS-NH_2 (0.1 mg mL^{-1}), the fluorescence intensity of the interface increases significantly with time, indicating the segregation and aggregation of the FPNPs at the interface. In a control experiment where there is no POSS-NH_2 in the toluene phase, no fluorescence is observed at the interface, further underscoring the integral role of NPS formation and assembly (Figure S5). With the enhanced interfacial activity of FPNPs, the Plateau−Rayleigh (PR) instabilities of water jets can be completely suppressed by jetting an aqueous FPNP solutions into silicone oil containing POSS-NH_2, enabling the generation of liquid tubules and the 3D printing of all-liquid constructs into programmed shapes (Figure S6). As shown in Figure 3b-c and Figure S7, by using a 3D printer to control the spatial arrangement of the liquids, an aqueous spiral with a fluorescent wall is prepared. However, in comparison to the reported liquid tubule with a straight wall, sugar-coated haws stick-like liquid tubule is obtained (Video S4). During the formation of liquid tubule, surface tension drives the breakup of the water jet and, due to the jamming of NPSs at the interface, the breakup is suppressed. If the particles are rigid, like inorganic NPs, the reorganization of particles at the interface will be difficult and, therefore, the shape of the liquids will be retained, as reported previously.[22-24] If the particles are soft, like FPNPs, the lateral compression driven by the reduction in the interfacial tension will deform FPNPs until balanced

by the elastic retractive force of the polymer chains in FPNPs. As a result, a shape evolution of the liquid tubule occurs, causing a wave-like interface (Figure 3c).

Figure 3. (a) LSCM images of water droplet containing FPNPs (0.05 mg mL^{-1}, pH = 3.0) in toluene solution containing POSS-NH_2 (0.1 mg mL^{-1}) over time. (b) Photographs of the sugar-coated haws stick-like liquid tubule in silicone oil under daylight and UV light. (c) Illustration of the formation of the special liquid tubule by 3D printing. [FPNP] = 1.0 mg mL^{-1}, [POSS-NH_2] = 30 mg mL^{-1}.

According to the soft nature of the FPNPs, more dense packing of the FPNPs can be achieved, leading to the fabrication of robust colloidosomes by sintering (Figure 4a). To produce colloidosomes, stable water-in-oil emulsions are prepared first by homogenizing the mixture of FPNP-containing glycerol/H_2O (50/50, v/v) solution and POSS-NH_2-containing vegetable oil/toluene (50/50, v/v) solution (Figure S8 and S9). After heating emulsion samples at 105 ^oC for 30 min, above the glass transition temperature (T_g) of the FPNPs (Figure S10), the polymer

chains in the FPNPs will interdiffuse, interconnecting the NPSs, resulting in water-in-oil colloidosomes. These colloidosomes can be transferred to a water continuous phase by gentle centrifugation and removal of the oil phase, and the integrity of the colloidosomes is retained (Figure 4b and 4c). Scanning electron microscopy (SEM) images show FPNPs are embedded within the walls of the colloidosomes (Figure 4d). Taking advantages of the carboxylic FPNPs, the permeability of the obtained colloidosomes can be triggered by the external stimulus, i.e., pH. Using fluorescein isothiocyanate (FITC) as a model cargo, the encapsulation and release behaviors of colloidosomes were investigated at different pH values. As shown in Figure 4e and 4f, a pH-responsive cargo release is obtained. With increasing pH, more cargo is released in a short time, due to the increased number of deprotonated carboxylic acid groups in the FPNPs. As a result, the polymer chains in the FPNPs repel each other, swelling the shell of the colloidosomes and accelerating the cargo release (Figure 4g and Figure S11).

Figure 4. (a) Schematic illustration of the preparation of the colloidosomes. (b) Optical and (c) fluorescent images of the colloidosome in water captured by LSCM. (d) SEM image of the colloidosomes. (e) Fluorescent image of the colloidosomes encapsulating FITC. (f) The pH-responsive cargo release of the colloidosomes. (g) pH-dependent swelling/shrinking of the colloidosomes. [FPNP] = 1.0 mg mL^{-1}, [POSS-NH_2] = 0.5 mg mL^{-1}, [FITC] = 0.05 mg mL^{-1}, sintering time: 30 min.

CONCLUSION

In conclusion, we have described the formation, assembly and jamming of a new type of NPS, by taking advantage of the electrostatic interactions between FPNP and POSS-NH_2 at the oil-water interface. Benefiting from the fluorescence of the FPNPs, the formation and assembly

processes of NPSs can be visualized in real-time. Due to the soft nature of FPNPs, upon application of compression, NPS assemblies can reorganize, relaxing in-plane stresses, and the distinctive self-assembly behaviors are displayed using all-liquid 3D printing. Sugar-coated haws stick-like liquid tubules encapsulated with jammed NPSs are obtained. By using NPS-stabilized Pickering emulsions as templates, pH-responsive colloidosomes are produced via thermal annealing. These results present a simple avenue for the construction of programmable liquid devices and controlled release delivery systems.

EXPERIMENTAL SECTION

Materials Fluorescent polymeric nanoparticles (FPNPs, 200 nm) were synthesized according to previous report.[34] Amine-terminated polyhedral oligomeric silsesquioxane (POSS-NH_2, M_w = 1267 g mol^{-1}) was purchased from Hybrid Plastics. Fluorescein isothiocyanate (FITC, 96%, Macklin) was used as received without further purification. Other reagents and solvents were purchased from Sigma-Aldrich and used as received except for additional declaration.

Characterization The interfacial tension (γ) was analyzed by a multi-functional tensiometer (Krüss DSA30) using a pendent drop method, where the evolution of γ with time was recorded after the aqueous phase was slowly injected into the oil phase. Droplet deformation and fluid flow were recorded as an image or video with a digital camera native to the tensiometer. The morphologies of emulsions were characterized by polarized optical microscopy (ZEISS Imager.A2) or confocal laser scanning microscope (Leica SP8). The morphologies of colloidosomes characterized by scanning electron microscope (SEM, Hitachi S-4700). The size distributions of molecules were characterized by dynamic light scattering (DLS, Malvern) at 298 K.

All-liquid 3D Printing [24] A commercially available JGAURORA 3D printer was modified to produce water-in-oil tubules. The print head nozzle was replaced by a stainless steel syringe needle and attached to a syringe pump. The trajectories of the print head were controlled by G-Code commands using software of Repetier-Host and 3ds Max. Depending on the desired feature sizes, the print head velocity was 300 ~ 700 mm min^{-1} and the FPNPs aqueous solutions were injected at a flow rate of 0.5 ~ 1.0 mL min^{-1}.

Fabrication of Water in Oil Colloidosomes [8] FPNPs (1.0 mg mL^{-1}, 200 μL) are dissolved in a mixture of glycerol/H_2O (50/50, v/v), POSS-NH_2 (0.5 mg mL^{-1}, 1200 μL) is dissolved in a mixture of vegetable oil/toluene (50/50, v/v) solution, then mixed the solutions in a 5.0 mL centrifuge tube by a high shear mixer at 10000 r min^{-1} for 1.0 min to obtain the water in oil Pickering emulsion. Then the Pickering emulsions were heated at 105 ° C for 30 minutes to sinter the interface. After that, emulsions were left for one day at ambient conditions to allow the microcapsules to sediment. The white sediment was then transferred into an empty centrifuge tube and washed with toluene and MilliQ water (18.2 MΩ cm), respectively. The mixture was centrifuged at 10000 rpm for 5.0 min at 25°C. The creamed oil was removed via pipetting, and the microcapsules were redispersed in an aqueous phase to further characterization.

Cargo Release Test The model cargo release was carried out using the dialysis bag method. Briefly, 2.0 mL colloidosomes loaded with FITC were transferred into a dialysis bag (MWCO 2000, Yuanye Bio-Technology, China) to form a hermetic pouch and then completely immersed in 48 mL of release medium (phosphate buffer with continuous stirring at 500 rpm. The dialysis membrane molecular weight cut-off was chosen on the basis of cargo molecular weight. Cargo release was assessed by intermittently sampling the contents (400 μL) of the medium. The equal fresh release medium was supplemented immediately after sampling. The collected samples were

analyzed by a fluorescence microplate reader (Fluoroskan Ascent, Thermo Scientific, Waltham, USA). The actual concentration of FITC in each sample was calculated using a calibration curve plotted by FITC standard solutions. The measured amount of cargo at each preset interval was converted into cumulative release.

ASSOCIATED CONTENT

Supporting Information. The following files are available free of charge.

DLS analysis and SEM images of the FPNPs; interfacial tension between POSS-NH_2 toluene solution and water with different pH values; water contact angles of 2D self-assembly films; LSCM images of water droplet containing FPNPs surrounded by pure toluene without containing POSS-NH_2; snapshot of suppressed PR instability; images of the liquid tubules and emulsion droplet and proofs for their stabilities; DSC curve of FPNPs; and pH responsibility of FPNPs detected by DLS (PDF)

Video showing the morphology evolution of droplets under compression (MP4)

Video showing the all-liquid 3D printing (MP4)

AUTHOR INFORMATION

Corresponding Authors

Guan Wang - Beijing Advanced Innovation Center for Soft Matter Science and Engineering, Beijing University of Chemical Technology, Beijing 100029, China, wangguan@buct.edu.cn

Shaowei Shi - Beijing Advanced Innovation Center for Soft Matter Science and Engineering, Beijing University of Chemical Technology, Beijing 100029, China, shisw@mail.buct.edu.cn

Xinggui Gu - Beijing Advanced Innovation Center for Soft Matter Science and Engineering, Beijing University of Chemical Technology, Beijing 100029, China; Beijing National Laboratory for Molecular Sciences, Beijing, 100190, China, guxinggui@mail.buct.edu.cn

ORCID

Guan Wang: 0000-0002-0317-5055

Shaowei Shi: 0000-0002-9869-4340

Xinggui Gu: 0000-0002-1678-2823

ACKNOWLEDGMENT

This work was supported by the National Natural Science Foundation of China (52173018, 52003023, 52173154, and 51988102). X. Gu acknowledges Beijing National Laboratory for Molecular Sciences (BNLMS202103). B. Z. Tang acknowledges the financial support from the National Science Foundation of China (21788102). TPR was supported by the U.S. Department of Energy, Office of Science, Office of Basic Energy Sciences, Materials Sciences and Engineering Division under Contract No. DE-AC02-05-CH11231 within the Adaptive Interfacial Assemblies Towards Structuring Liquids program (KCTR16) and the Army Research Office under contract W911NF-20-0093.

REFERENCES

1. Whitesides. M.; Grzybowski, B., Self-Assembly at All Scales. *Science* **2002,** *295*, 2418-2421.

2. Whitesides. M.; Boncheva, M., Beyond Molecules: Self-Assembly of Mesoscopic and Macroscopic Components. *PNAS* **2002,** *99*, 4769-4774.

3. Binks, B. P., Particles as surfactants - Similarities and Differences. *Curr. Opin. Colloid Interface Sci.* **2002,** *7*, 21-41.

4. Chevalier, Y.; Bolzinger, M.A., Emulsions Stabilized with Solid Nanoparticles: Pickering Emulsions. *Colloids Surf. A Physicochem. Eng. Asp.* **2013,** *439*, 23-34.

5. Ni, L.; Yu, C.; Wei, Q.; Liu, D.; Qiu, J., Pickering Emulsion Catalysis: Interfacial Chemistry, Catalyst Design, Challenges, and Perspectives. *Angew. Chem. Int. Ed.* **2022,** *61*, e202115885.

6. Pickering, S. U., CXCVI.—Emulsions. *J. Chem. Soc., Trans.* **1907,** *91*, 2001-2021.

7. Thompson, K. L.; Williams, M.; Armes, S. P., Colloidosomes: Synthesis, Properties and Applications. *J. Colloid Interface Sci.* **2015,** *447*, 217-228.

8. Dinsmore, A. D.; Hsu, M. F.; Nikolaides, M. G.; Marquez, M.; Bausch, A. R.; Weitz, D. A., Colloidosomes: Selectively Permeable Capsules Composed of Colloidal Particles. *Science* **2002,** *298*, 1006-1009.

9. Hsu, M. F.; Nikolaides, M. G.; Dinsmore, A. D.; Bausch, A. R.; Gordon, V. D.; Chen, X.; Hutchinson, J. W.; Weitz, D. A.; Marquez, M., Self-assembled Shells Composed of Colloidal Particles: Fabrication and Characterization. *Langmuir* **2005,** *21*, 2963-2970.

10. Shi, S.; Russell, T. P., Nanoparticle Assembly at Liquid-Liquid Interfaces: From the Nanoscale to Mesoscale. *Adv. Mater.* **2018,** *30*, e1800714.

11. Lin, Y.; Skaff, H.; Emrick, T.; Dinsmore, A. D.; Russell, T. P., Nanoparticle Assembly and Transport at Liquid-Liquid Interfaces. *Science* **2003,** *299*, 226-229.

12. Pieranski, P., Two-Dimensional Interfacial Colloidal Crystals. *Phys. Rev. Lett.* **1980,** *45*, 569-572.

13. Shao, Y.; Ye, Y.; Sun, D.; Yang, Z., Polymer-Derived Janus Particles at Multiple Length Scales. *Macromolecules* **2022,** *55*, 6297-6310.

14. Lattuada, M.; Hatton, T. A., Synthesis, Properties and Applications of Janus Nanoparticles. *Nano Today* **2011,** *6*, 286-308.

15. Liu, Y.; Wang, J.; Shao, Y.; Deng, R.; Zhu, J.; Yang, Z., Recent Advances in Scalable Synthesis and Performance of Janus Polymer/Inorganic Nanocomposites. *Prog. Mater Sci.* **2022,** *124*, 100888.

16. Shao, Y.; Yang, Z., Progress in Polymer Single-Chain Based Hybrid Nanoparticles. *Prog. Polym. Sci.* **2022,** *133*, 101593.

17. Cui, M.; Emrick, T.; Russell, T. P., Stabilizing Liquid Drops in Nonequilibrium Shapes by the Interfacial Jamming of Nanoparticles. *Science* **2013,** *342*, 460-463.

18. Sun, S.; Liu, T.; Shi, S.; Russell, T. P., Nanoparticle surfactants and structured liquids. *Colloid. Polym. Sci.* **2021,** *299*, 523-536.

19. Yang, Y.; Xia, Z.; Luo, Y.; Wu, Z.; Shi, S.; Russell, T. P., Reconfigurable structured liquids. *Supramol. Mater.* **2022,** *1*, 100013.

20. Li, Y.; Liu, X.; Zhang, Z.; Zhao, S.; Tian, G.; Zheng, J.; Wang, D.; Shi, S.; Russell, T. P., Adaptive Structured Pickering Emulsions and Porous Materials Based on Cellulose Nanocrystal Surfactants. *Angew. Chem. Int. Ed.* **2018,** *57*, 13560-13564.

21. Shi, S.; Qian, B.; Wu, X.; Sun, H.; Wang, H.; Zhang, H. B.; Yu, Z. Z.; Russell, T. P., Self-Assembly of MXene-Surfactants at Liquid-Liquid Interfaces: From Structured Liquids to 3D Aerogels. *Angew. Chem. Int. Ed.* **2019,** *58*, 18171-18176.

22. Sun, H.; Li, M.; Li, L.; Liu, T.; Luo, Y.; Russell, T. P.; Shi, S., Redox-Responsive, Reconfigurable All-Liquid Constructs. *J. Am. Chem. Soc.* **2021,** *143*, 3719-3722.

23. Liu, T.; Yin, Y.; Yang, Y.; Russell, T. P.; Shi, S., Layer-by-Layer Engineered All-Liquid Microfluidic Chips for Enzyme Immobilization. *Adv. Mater.* **2022,** *34*, 2105386.

24. Forth, J.; Liu, X.; Hasnain, J.; Toor, A.; Miszta, K.; Shi, S.; Geissler, P. L.; Emrick, T.; Helms, B. A.; Russell, T. P., Reconfigurable Printed Liquids. *Adv. Mater.* **2018,** *30*, e1707603.

25. Shi, S.; Liu, X.; Li, Y.; Wu, X.; Wang, D.; Forth, J.; Russell, T. P., Liquid Letters. *Adv. Mater.* **2018,** *30*, 1705800.

26. Liu, X.; Shi, S.; Li, Y.; Forth, J.; Wang, D.; Russell, T. P., Liquid Tubule Formation and Stabilization Using Cellulose Nanocrystal Surfactants. *Angew. Chem. Int. Ed.* **2017,** *56*, 12594-12598.

27. Feng, W.; Chai, Y.; Forth, J.; Ashby, P. D.; Russell, T. P.; Helms, B. A., Harnessing Liquid-in-liquid Printing and Micropatterned Substrates to Fabricate 3-Dimensional All-liquid Fluidic Devices. *Nat. Commun.* **2019,** *10*, 1095.

28. Sun, H. L.; Li, L. S.; Russell, T. P.; Shi, S. W., Photoresponsive Structured Liquids Enabled by Molecular Recognition at Liquid-Liquid Interfaces. *J. Am. Chem. Soc.* **2020,** *142*, 3719-3722.

29. Wang, B.; Liu, T.; Chen, H.; Yin, B.; Zhang, Z.; Russell, T. P.; Shi, S., Molecular Brush Surfactants: Versatile Emulsifiers for Stabilizing and Structuring Liquids. *Angew. Chem. Int. Ed.* **2021,** *60*, 19626-19630.

30. Sun, S.; Luo, Y.; Yang, Y.; Chen, J.; Li, S.; Wu, Z.; Shi, S., Supramolecular Interfaces and Reconfigurable Liquids Derived from Cucurbit[7]uril Surfactants. *Small* **2022,** *n/a*, 2204182.

31. Xia, Z.; Lin, C.-G.; Yang, Y.; Wang, Y.; Wu, Z.; Song, Y.-F.; Russell, T. P.; Shi, S., Polyoxometalate-Surfactant Assemblies: Responsiveness to Orthogonal Stimuli. *Angew. Chem. Int. Ed.* **2022,** *61*, e202203741.

32. Luo, Y.; Yang, Y.; Wang, Y.; Wu, Z.; Russell, T. P.; Shi, S., Reconfigurable Liquids Constructed by Pillar[6]arene-Based Nanoparticle Surfactants. *Angew. Chem. Int. Ed.* **2022,** *61*, e202207199.

33. Wang, G.; Zhou, L.; Zhang, P.; Zhao, E.; Zhou, L.; Chen, D.; Sun, J.; Gu, X.; Yang, W.; Tang, B. Z., Fluorescence Self-Reporting Precipitation Polymerization Based on Aggregation-Induced Emission for Constructing Optical Nanoagents. *Angew. Chem. Int. Ed.* **2020,** *59*, 10122-10128.

34. Wang, G.; Yang, L.; Li, C.; Yu, H.; He, Z.; Yang, C.; Sun, J.; Zhang, P.; Gu, X.; Tang, B. Z., Novel Strategy to Prepare Fluorescent Polymeric Nanoparticles Based on Aggregation-Induced Emission via Precipitation Polymerization for Fluorescent Lateral Flow Assay. *Mater. Chem. Front.* **2021,** *5*, 2452-2458.

35. Kang, M.; Zhang, Z.; Song, N.; Li, M.; Sun, P.; Chen, X.; Wang, D.; Tang, B. Z., Aggregation-Enhanced Theranostics: AIE Sparkles in Biomedical Field. *Aggregate* **2020,** *1*, 80-106.

36. Zhao, X.; Alam, P.; Zhang, J.; Lin, S.; Peng, Q.; Zhang, J.; Liang, G.; Chen, S.; Zhang, J.; Sung Herman, H. Y.; Lam Jacky, W. Y.; Williams Ian, D.; Gu, X.; Zhao, Z.; Tang Ben, Z., Metallophilicity-Induced Clusterization: Single-Component White-Light Clusteroluminescence with Stimulus Response. *CCS Chem.* **2021,** *3*, 3039-3049.

37. Luo, J.; Xie, Z.; Lam, J. W. Y.; Cheng, L.; Chen, H.; Qiu, C.; Kwok, H. S.; Zhan, X.; Liu, Y.; Zhu, D.; Tang, B. Z., Aggregation-induced Emission of 1-methyl-1,2,3,4,5-pentaphenylsilole. *Chem. Commun.* **2001,** 1740-1741.

38. Mei, J.; Leung, N. L. C.; Kwok, R. T. K.; Lam, J. W. Y.; Tang, B. Z., Aggregation-Induced Emission: Together We Shine, United We Soar! *Chem. Rev.* **2015,** *115*, 11718-11940.

39. Li, L.; Ma, H.; Zhang, J.; Zhao, E.; Hao, J.; Huang, H.; Li, H.; Li, P.; Gu, X.; Tang, B. Z., Emission-Tunable Soft Porous Organic Crystal Based on Squaraine for Single-Crystal Analysis of Guest-Induced Gate-Opening Transformation. *J. Am. Chem. Soc.* **2021,** *143*, 3856-3864.

40. Qian, B.; Shi, S.; Wang, H.; Russell, T. P., Reconfigurable Liquids Stabilized by DNA Surfactants. *ACS Appl. Mater. Interfaces* **2020,** *12*, 13551-13557.

41. Xu, R.; Liu, T.; Sun, H.; Wang, B.; Shi, S.; Russell, T. P., Interfacial Assembly and Jamming of Polyelectrolyte Surfactants: A Simple Route To Print Liquids in Low-Viscosity Solution. *ACS Appl. Mater. Interfaces* **2020,** *12*, 18116-18122.

Table of Contents